

# Full-Duplex Radios for Edge Caching

Italo Atzeni and Marco Maso

**Abstract** Recent studies have shown that edge caching may have a beneficial effect on the sustainability of future wireless networks. While its positive impact at the network level is rather clear (in terms of, e.g., access delay and backhaul load), assessing its potential benefits at the physical layer is less straightforward. This chapter builds upon this observation and focuses on the performance enhancement brought by the addition of caching capabilities to full-duplex (FD) radios in the context of ultra-dense networks (UDNs). More specifically, we aim at showing that the interference footprint of such networks, i.e., the major bottleneck to overcome to observe the theoretical FD throughput doubling at the network level, can be significantly reduced thanks to edge caching. As a matter of fact, fundamental results available in the literature show that most of the gain, as compared to their half-duplex (HD) counterparts, can be achieved by such networks only if costly modifications to their infrastructure are performed and/or if high-rate signaling is exchanged between user equipments (UEs) over suitable control links. Therefore, we aim at proposing a viable and cost-effective alternative to these solutions based on pre-fetching locally popular contents at the network edge. We start by considering an interference-rich scenario such as an ultra-dense FD small-cell network, in which several non-cooperative FD base stations (BSs) serve their associated UEs while communicating with a wireless backhaul node (BN) to retrieve the content to deliver. We then describe a geographical caching policy aiming at capturing local files popularity and compute the corresponding cache-hit probability. Thereupon, we calculate the probability of successful transmission of a file requested by a UE, either directly by its serving small-cell base station (SBS) or by the corresponding BN: this quantity is then used to lower-bound the throughput of the considered network. Our approach leverages tools from stochastic geometry in order to guarantee both analytical tractability of the problem and generality of the results. A set of suitable numerical simulations is finally performed to confirm the correctness of the theoretical findings and characterize the performance enhancement brought by the adoption of edge caching. The most striking result in this sense is the remarkable performance improvement observed when shifting from cache-free to cache-aided FD small-cell networks.

---

Italo Atzeni  
Communication Systems Department, EURECOM, Sophia Antipolis, France.  
e-mail: [italo.atzeni@ieee.org](mailto:italo.atzeni@ieee.org)  
Marco Maso  
Nokia Bell Labs, Paris-Saclay, France.  
e-mail: [marco.maso@nokia.com](mailto:marco.maso@nokia.com)

## 1 Introduction

The last decade has witnessed the progressive introduction of the fourth generation (4G) cellular network technology and the concurrent adoption of increasingly competitive pricing strategies by device manufacturers and telcos. As a consequence, devices that are able to offer reliable broadband data connections to their users, i.e., smartphones, ceased to be premium products and became a commodity. Their market penetration is already massive and keeps progressing at steady pace. Recent studies forecast that smartphones will represent 86% of the total mobile data traffic by 2021, compared to 81% in 2016, and that monthly mobile data traffic will reach 49 exabytes worldwide (or, equivalently, a run rate of 587 exabytes annually) [1].

The amount of network resources needed to support these trends is ever-increasing. Telcos already anticipate that current mobile networks will have to be restructured to cope with both future service demands and the multitude of novel mobile broadband applications constantly introduced in the market. Many important requirements have been identified in this context, such as the need for higher spectral and energy efficiency, lower end-to-end delays, better coverage, large scalability, and lower capital expense (CAPEX) and operating expenses (OPEX), just to name a few [2]. As a consequence, one of the strongest drivers in the last years for several research groups in both industry and academia has been the need to define a more advanced and flexible network technology as compared to 4G, i.e., the so-called fifth generation (5G). The remarkable results of such activities have already yielded significant outcomes within standardization development organizations like the 3rd Generation Partnership Project (3GPP), who have already published the first version of the standard that will guide the deployment of future 5G wireless networks, i.e., 3GPP Release 15 [3, 4]. This evolution, conventionally referred to as New Radio (NR), is planned to hit the market in its non-standalone version within 2019, and is expected to provide significant gains over previous systems.

From a practical point of view, NR deployments will be characterized by the introduction, or further development, of several key solutions expected to bring the sought performance enhancement as compared to existing networks. Interestingly, only some strategies and network configurations have been and are subject to standardization, whereas some others are considered as part of the implementation aspects. Noteworthy and representative examples of these two categories are [3, 4]:

- *Massive multiple-input multiple-output (MIMO)*: this natural candidate for the physical layer of NR has imposed a revision of the reference sequences and channel state information (CSI) feedback mechanisms [5, 6];
- *Advanced MIMO precoding*: the adoption of such strategies at the base station (BS) should be completely transparent to the UE, i.e., precoding solutions are implementation aspects that are not specified in the standard.

As a matter of fact, the relevance and impact of many other technologies and approaches will increase in future 5G networks as compared to their current role in mobile and fixed networks, regardless of their 3GPP standardization status (i.e., specified or not). In this chapter, we specifically focus on two of these approaches to study and discuss the potential brought by their mutual interactions:

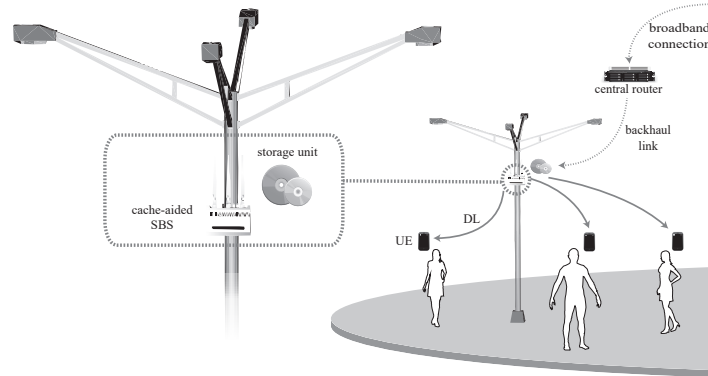


**Fig. 1** Cache-aided SBS: the SBS is equipped with a storage unit to pre-fetch popular content.

- The so-called *proactive caching* at the network edge, by means of which contents (e.g., videos, images, and news) are brought closer to the users and intelligently cached at SBSs equipped with high-capacity storage units, as illustrated in Fig. 1. As a result, the end-to-end access delay is significantly reduced, the mobile infrastructure is offloaded, and the impact of limited-capacity backhaul on the network performance is mitigated [7–12]. The role of edge caching becomes particularly crucial in case of UDN deployments, i.e., massively populated (and possibly heterogeneous) networks in which the distance between BSs and served UEs is reduced as compared to classic macro-cell networks [13–16]. Such UDNs may comprise several layers, each of them including different categories of cells (i.e., femto, pico, micro, and macro cells) [17–19]. In general, this layered architecture allows to design efficient strategies to offload the pre-existing macro-cell infrastructure and enhance the network capacity, especially when several nodes provide caching support [20].
- The transition from HD to *FD operations* at radio terminals also promises to offer many benefits, although subject to some peculiar limitations [21–25]. A FD device does not require separate time/frequency resources to be able to support data transmission and reception. In other words, it can simultaneously transmit and receive data over the same bandwidth, thus having the potential to achieve a theoretical throughput doubling and energy efficiency enhancement in comparison to HD radios. In particular, equipping network nodes with FD capabilities can simplify the adoption of flexible duplexing strategies such as dynamic time-division duplexing (TDD) and enable readjustments to frame structures on-the-fly. Additionally, FD transmission offers advantages in terms of operation, cost, and efficiency as compared to traditional HD operating mode [26].

The aforementioned approaches certainly have significant potential if taken individually. Nevertheless, assessing the extent of their interoperability is not straightforward. This is mostly due to the interference footprint of the FD links [24], which may complicate a seamless integration of caching capabilities at each network nodes. At this stage, a brief introduction of such technology is in order, to better characterize its features and

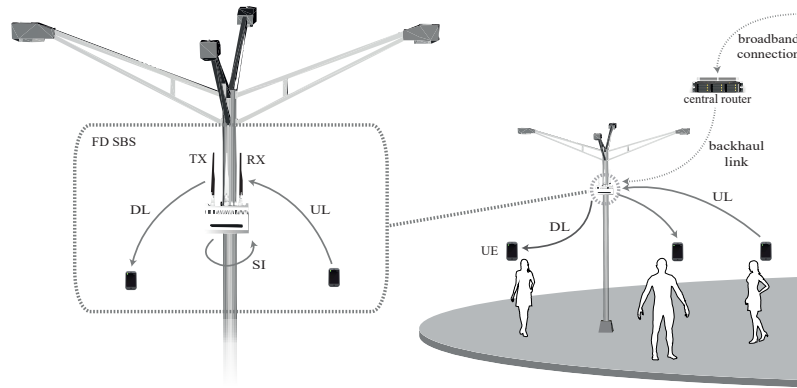


**Fig. 2** FD SBS: data transmission and reception occur in the same time/frequency resource.

issues, before studying the impact of edge caching on the performance of FD radios and networks.

### 1.1 Full Duplex Communications

The majority of current wireless radios operate in HD mode. In practice, these devices perform data transmission and reception over separate time/frequency resources. Depending on the way such resources are used, we can have either TDD or frequency-division duplexing (FDD) operations, i.e., uplink (UL) and downlink (DL) transmissions occur over two different time or frequency resources, respectively. This approach has several advantages in terms of both ease of implementation and rather straightforward network operations to perform multi-cell transmissions. As a matter of fact, it can be argued that this implicitly sets a hard constraint on the spectral efficiency of the system. For this reason, many research efforts have been performed lately to investigate the potential and the feasibility of FD communications, in which the same time/frequency resource is used to perform the UL and DL data transmissions. However, the strong self-interference (SI) observed by the FD radio during the signal reception enforces a crucial obstacle to the feasibility of such approach. In other terms, a non-negligible portion of the transmitted signal is always received by the device's receive chain, in turn reducing the signal-to-interference-plus-noise ratio (SINR) of the incoming useful signals [27–29]. This situation is schematically depicted in Fig. 2. Many different transceiver designs and self-interference cancellation (SIC) algorithms have been devised to ensure the feasibility of FD operations [28–38]. These solutions can be classified into two major categories based on passive or active cancellation. In the former case, SIC is achieved in the propagation domain by physical separation of the transmit and receive antennas. Conversely, active SIC solutions exploit the FD node's knowledge of its own transmitted signal to subtract it from the receive signal after appropriate manipulations and processing.

Unfortunately, the SI is not the only problem that system designers must face when dealing with FD radios. The major obstacle to their practical adoption in future 5G networks is arguably the aggregated interference footprint resulting from multiple and concurrent FD communications within the network. Let us provide an example to highlight this issue. Consider a simple network composed of several FD nodes arranged in BS/UE pairs and take an active BS/UE pair as reference. During UE-to-BS UL operations, every neighboring BS engaging in DL transmission strongly interferes with the considered BS, inducing the so-called *BS-to-BS interference*. Similarly, during BS-to-UE DL operations, all the UEs performing UL transmission heavily interfere with the considered UE, creating the so-called *UE-to-UE interference*, also referred to as inter-node interference (INI) [39, 40]. In practice, the FD throughput gain tends to 2 in case of very sparse deployment of nodes. Nevertheless, such gain saturates quickly as the network density increases, the fundamental reason being that the number of interfering nodes also doubles with respect to the HD case. This becomes more significant when either the link distance decreases or the node density increases [41]. In other words, the theoretical throughput doubling brought by FD at the device level does not seem to materialize straightforwardly at the network level (regardless of the effectiveness of the adopted SIC algorithms), unless specific and possibly costly countermeasures are taken. As a result, the aggressive spatial frequency reuse inherent to dense network deployments may not be feasible due to the presence of a multitude of FD links mutually interfering at all times.

Studies and analysis of the FD interference footprint have been recently carried out to identify viable strategies to reduce it and improve the scalability of the FD throughput enhancement. A myriad of approaches has been proposed to address this problem; indeed they range from user scheduling algorithms to advanced interference management and power control techniques. A common feature shared by such solutions is that they require the adoption of additional signaling among nodes or the implementation of heavy infrastructural changes [24, 25, 38–40, 42, 43]. In this context, two fundamental results can be highlighted: on the one hand, it is shown in [24] that most of the theoretical network throughput gain is achievable if only the BSs operate in FD while the UEs operate in HD, and centralized scheduling decisions are taken by a central unit enjoying full access to global system information; on the other hand, it is shown in [43] that, in case of distributed network control and operations, FD gains can be observed only if the UEs can exchange suitable information about INI over one or more orthogonal control links. Hence, the relevance of the aforementioned results is mostly theoretical, as the advocated infrastructural changes at the network level are extremely expensive. One of the goals of this chapter is to investigate the feasibility of a constructive alternative to such approaches: this considers the interactions between FD operations and smart caching strategies, and avoids any substantial changes to the network infrastructure and to the signaling exchange among nodes.

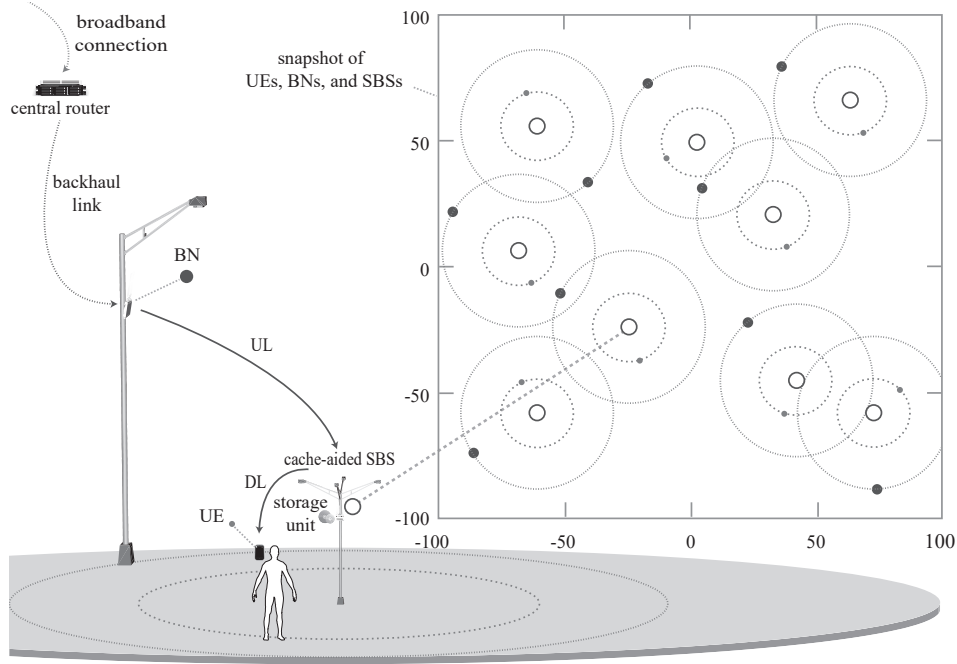


Fig. 3 Snapshot of the marked PPP modeling the SBSs, UL nodes, and DL nodes.

## 2 System Model

### 2.1 Network Model

Consider a UDN comprising: *i*) a tier of macro-cell BNs equipped with internet access, *ii*) a tier of SBSs providing network coverage, and *iii*) a set of mobile UEs. Each SBS communicates with only one BN in the UL direction and transmits contents to only one UE in the DL direction, functioning as a relay between the two. The SBSs operate in FD, whereas both BNs and UEs operate in HD mode; the same time/frequency resource is used for the communications in both directions. In the following, and focusing our attention on the SBSs, the BNs and the UEs are referred to as *UL nodes* and *DL nodes*, respectively.

Spatial random models allow to seize the randomness of realistic ultra-dense small-cell deployments and, in addition, to derive tractable and accurate expressions for system-level performance analysis [44]. Therefore, we model the spatial distribution of the network nodes (i.e., SBSs and UL/DL nodes) using the homogeneous, independently marked Poisson point process (PPP)  $\Phi \triangleq \{(x, u(x), d(x))\} \subset \mathbb{R}^2 \times \mathbb{R}^2 \times \mathbb{R}^2$ . Here, we let  $\Phi_{\text{SBS}} \triangleq \{x\}$  denote the ground PPP of the SBSs with spatial density  $\lambda$  (measured in [SBSs/m<sup>2</sup>]), whereas the isotropic marks  $\Phi_{\text{UL}} \triangleq u(\Phi_{\text{SBS}}) = \{u(x)\}_{x \in \Phi_{\text{SBS}}}$  and  $\Phi_{\text{DL}} \triangleq d(\Phi_{\text{SBS}}) = \{d(x)\}_{x \in \Phi_{\text{SBS}}}$  denote the PPPs of the UL and DL nodes, respectively. Further-

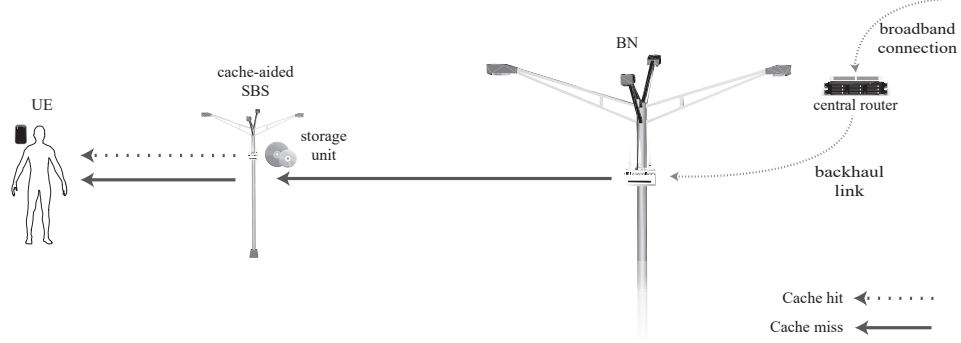


**Fig. 4** Communication links in case of cache hit and cache-miss.

more, let  $r_{y,z} \triangleq \|y - z\|$  be the distance between nodes  $y, z \in \Phi$ ; the distances of the UL and DL nodes from their associated SBSs are assumed fixed and are denoted by  $R_{UL} \triangleq r_{u(x),x}$  and  $R_{DL} \triangleq r_{x,d(x)}$ ,  $\forall x \in \Phi_{SBS}$ , respectively. It is thus evident that, according to these definitions, the PPPs  $\Phi_{UL}$  and  $\Phi_{DL}$  are dependent on the ground PPP  $\Phi_{SBS}$  and have the same spatial density of the latter. Lastly, since the SBSs cover small areas compared with the BNs, one can reasonably assume that  $R_{UL} \gg R_{DL}$ . A snapshot of the considered two-tier network is given in Fig. 3.

## 2.2 Cache-aided Network Nodes

Let us assume that the UL nodes have direct access to the *global file catalog*  $\mathcal{F} \triangleq \{f_1, f_2, \dots, f_F\}$ , with  $|\mathcal{F}| = F$ , which can be interpreted as a subset of all the contents available on the internet. Without loss of generality, we assume that all files have identical length, as files with different lengths can be always split into chunks of equal size. In this context, whenever a DL node sends a request for a content in  $\mathcal{F}$ , its serving SBS, operating in FD mode, fetches the corresponding file from the associated UL node and delivers it to the DL node. In UDN scenarios, however, the reliability of the content transmission may be reduced by the aggressive spatial frequency reuse, which may sensibly diminish the throughput with respect to an equivalent HD network.

Assume that SBS  $x \in \Phi_{SBS}$  is equipped with a *storage unit*  $\Delta_x$  with size  $S < F$  files and that DL node  $d(x)$  sends a request for file  $f_i \in \mathcal{F}$ . Let  $\mathcal{P} \triangleq \{p_1, p_2, \dots, p_F\}$ , with  $\sum_{i=1}^F p_i = 1$ , be the set of request probabilities of each file, which depends on the files popularity over the whole network. Now, a *cache-hit* event occurs whenever  $f_i \in \Delta_x$ , i.e., if  $f_i$  is cached at SBS  $x$ . In this case, DL node  $d(x)$  is served directly by SBS  $x$  without any communication between SBS  $x$  and UL node  $u(x)$ ; alternatively, a *cache-miss* event occurs whenever  $f_i \notin \Delta_x$ , i.e., if  $f_i$  is not available in the cache, and SBS  $x$  must fetch the file from UL node  $u(x)$  and deliver it to  $d(x)$  in FD mode (see Fig. 4). Thus, a cache-hit event allows to offload the overlaying macro-cell infrastructure and, since the UL becomes inactive, removes the need for the SBS to operate in FD mode. As a consequence, two major

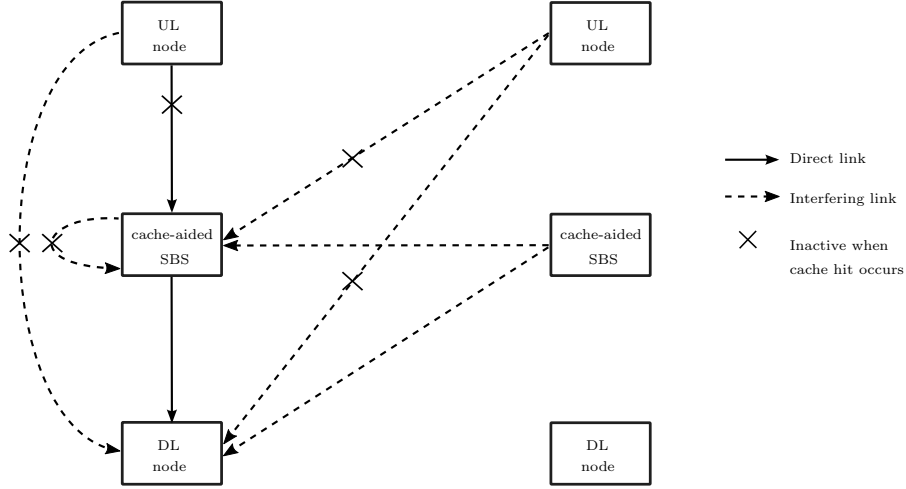


**Fig. 5** Adopted system model including cache-aided SBSs, UL nodes, and DL nodes, with corresponding direct and interfering links.

advantages can be observed in terms of reduced interference: *i*) at the single-cell level, both the SI (at the SBS) and the INI (at the DL node) disappear; *ii*) at the network level, the inter-cell interference is substantially reduced. Fig. 5 provides a schematic representation of the so-obtained scenario, whose interference terms are described in Section 2.4.

A key parameter to assess the effectiveness of the considered cache-aided approach is the so-called *cache-hit probability*, denoted by  $P_{\text{hit}}$ , which is the probability that any file requested by a given DL node is cached at its associated SBS. The framework adopted in this chapter to model such probability is presented in Section 3. In particular, such framework is designed to capture the local files popularity in non-cooperative random networks. Subsequently, we investigate the system-level performance gain brought by the deployment of cache-aided SBSs in FD networks for a given  $P_{\text{hit}}$  in Section 4.

### 2.3 Channel Model

In the considered system model, we assume that all nodes are single-antenna devices; the extension of our study to multi-antenna settings goes beyond the scope of this chapter and can be accomplished using the analytical framework presented in [25, 45]. In addition, it is assumed that the UL nodes and the SBSs transmit with powers  $\rho_{\text{UL}}$  and  $\rho_{\text{DL}}$ , respectively.

The wireless channel propagation is characterized as the combination of two main parameters, i.e., large-scale pathloss attenuation and small-scale fading. Let  $\ell(y, z) \triangleq r_{y,z}^{-\alpha}$  be the pathloss function between nodes  $y$  and  $z$ . We base our model upon the ITU-R urban micro-cellular (UMi) pathloss model described in [46], where different attenuations are specified for the links between different types of nodes. Accordingly, we let  $\alpha = \alpha_2$  if  $y \in \Phi_{\text{UL}} \wedge z \in \Phi_{\text{DL}}$  (i.e., between BNs and UEs) and  $\alpha = \alpha_1$  otherwise (i.e., between BNs



and SBSs as well as between SBSs and UEs). In this respect, we assume non-line-of-sight propagation between UL and DL nodes, which results in stronger pathloss attenuation as compared to the other links, and set  $\alpha_2 \geq \alpha_1 > 2$ . Switching the focus to the small-scale fading, let  $h_{y,z}$  denote the channel power fading gain between nodes  $y$  and  $z$ . We assume that the SI channel is subject to Rician fading [27], whereas all the other channels are subject to Rayleigh fading. In other terms, we have that  $h_{y,z} \sim \exp(1)$  if  $y \neq z$  and  $h_{y,y} \sim \Gamma(a, b)$ . In particular, the shape parameter  $a$  and scale parameter  $b$  of the SI distribution can be computed in closed form from the Rician  $K$ -factor  $K$  and the SI attenuation  $\Omega$  measured at the SBS when communicating in FD, as detailed in [25, Lem. 1].

## 2.4 Signal-to-Interference Ratio

Massive and dense small-cell deployments, such as the one considered in this chapter, are often characterized by heavy inter-cell interference as a result of the very short inter-site distance [25]. As a consequence, it is meaningful to specifically focus on the interference-limited regime, where the noise is overwhelmed by interference. In this context, the definition of an appropriate metric, such as the measured signal-to-interference ratio (SIR) at the SBSs and at the DL nodes, is paramount to be able to capture the essential features of the interference-limited regime. We start by denoting a cache-miss event at SBS  $x$  with the notation  $\mathbb{A}_x$  and accordingly define the indicator function

$$\mathbb{1}_{\mathbb{A}_x} \triangleq \begin{cases} 1, & \text{if } \mathbb{A}_x, \\ 0, & \text{otherwise.} \end{cases} \quad (1)$$

The SIR at SBS  $x$  may be written as

$$\text{SIR}_x \triangleq \frac{\rho_{\text{UL}} R_{\text{UL}}^{-\alpha_1} h_{u(x),x}}{I_x} \quad (2)$$

with aggregate interference given by

$$I_x \triangleq \sum_{y \in \Phi_{\text{SBS}} \setminus \{x\}} (\rho_{\text{DL}} r_{y,x}^{-\alpha_1} h_{y,x} + \rho_{\text{UL}} r_{u(y),x}^{-\alpha_1} h_{u(y),x} \mathbb{1}_{\mathbb{A}_y}) + h_{x,x} \mathbb{1}_{\mathbb{A}_x} \quad (3)$$

is the interference term. Similarly, the SIR at DL node  $d(x)$  may be written as

$$\text{SIR}_{d(x)} \triangleq \frac{\rho_{\text{DL}} R_{\text{DL}}^{-\alpha_1} h_{x,d(x)}}{I_{d(x)}} \quad (4)$$

with aggregate interference given by

$$I_{d(x)} \triangleq \sum_{y \in \Phi_{\text{SBS}} \setminus \{x\}} (\rho_{\text{UL}} r_{y,d(x)}^{-\alpha_1} h_{y,d(x)} + \rho_{\text{DL}} r_{u(y),d(x)}^{-\alpha_1} h_{u(y),d(x)} \mathbb{1}_{\mathbb{A}_y}) + \rho_{\text{UL}} r_{u(x),d(x)}^{-\alpha_2} h_{u(x),d(x)} \mathbb{1}_{\mathbb{A}_x}. \quad (5)$$

The effect of equipping the SBSs with storage capabilities and shifting from a cache-free to a cache-aided scenario is rather evident upon observing (3) and (5). More precisely, a cache-hit event induces a reduction of the following major interference components, at both the network and the device level:

- Aggregate network interference;
- SI at the SBSs [27];
- INI at the DL nodes [39, 40].

We recall that the last two interference terms are the two main causes hindering the practical feasibility of FD technology at the network level.

### 3 Caching Model

A necessary step when performing studies on the performance of cache-aided networks is the definition of a caching model, whose role is to establish how files are requested and cached by DL nodes and SBSs, respectively [7]. Accordingly, this section introduces the non-cooperative, static caching model used throughout this chapter, which aims at mimicking a geographical caching policy based on local files popularity.<sup>1</sup> In this regard, it is important to note that existing literature typically does not consider geographical aspects of the files popularity of the UEs when defining caching models (we refer to [12] for an overview on content request models).

Here, the spatial distribution of the contents from the global file catalog  $\mathcal{F}$  is modeled by means of the homogeneous, independently marked PPP  $\Psi \triangleq \{(y, f(y))\} \subset \mathbb{R}^2 \times \mathcal{F}$ , where  $\Psi_{\mathcal{F}} \triangleq \{y\}$  is the PPP of the files with spatial density  $\eta$  (measured in [files/m<sup>2</sup>]). In this context, each file  $f_i \in \mathcal{F}$  corresponds to a thinned PPP with spatial density  $p_i \eta$ . Moreover, we assume that the files in  $\mathcal{F}$  are ordered by decreasing popularity, i.e.,  $p_1 \geq p_2 \geq \dots \geq p_F$ . The considered caching model consists of two core concepts, i.e., the *request region* and the *caching policy*, which describe how DL nodes request files and how SBSs cache files, respectively. The introduction of a last notation is in order to be able to explicitly add a geographical dimension to these two concepts. Accordingly, we let  $\mathcal{B}(z, \nu)$  denote the ball of radius  $\nu$  (measured in [m]) centered at node  $z \in \Phi_{\text{SBS}} \cup \Phi_{\text{DL}}$ .

**Definition 1 (Request region).** Assume that DL node  $d(x) \in \Phi_{\text{DL}}$  is interested in requesting locally popular files. Then, the request region of DL node  $d(x)$  is defined as

$$\mathcal{R}_{d(x)} \triangleq \{\Psi_{\mathcal{F}} \cap \mathcal{B}(d(x), R_{\text{R}})\} \quad (6)$$

with  $R_{\text{R}}$  defined as the *radius* of the request region.

**Remark 1** *From a qualitative point of view,  $R_{\text{R}}$  is related to the local interests of the UEs with respect to globally requested files. In other terms, if DL node  $d(x)$  is interested*

---

<sup>1</sup> More complex cooperative caching policies can be devised. However, this goes beyond the scope of this chapter.

in requesting all possible files in the global file catalog  $\mathcal{F}$ , then  $R_R \rightarrow \infty$  (provided that  $\{p_i > 0\}_{i=1}^F$ ).

**Definition 2 (Caching policy).** Assume that SBS  $x \in \Phi_{\text{SBS}}$  is interested in caching locally popular files. Then, the potential cache region is defined as

$$\mathcal{C}_x \triangleq \{\Psi_{\mathcal{F}} \cap \mathcal{B}(x, R_C)\} \quad (7)$$

with  $R_C$  defined as the radius of the potential cache region. The caching policy of SBS  $x \in \Phi_{\text{SBS}}$  is defined as

$$\Delta_x \triangleq \{f_i : f_i \in \mathcal{C}_x \wedge i \leq S\}. \quad (8)$$

**Remark 2** SBSs operating according to such caching policy will cache only geographically close (and, therefore, popular) files, in turn aiming at reducing the overhead associated with pre-fetching files from the BNs.

**Remark 3** Similarly to what has been previously observed for the request region, as  $R_C \rightarrow \infty$ , we note that such caching policy will always converge to storing globally popular files as in [7].

Finally, the following Lemma formalizes the cache-hit probability under the described caching model.

**Lemma 1.** *The cache-hit probability is given by*

$$P_{\text{hit}} = \frac{1}{F} \sum_{i=1}^S (1 - e^{-p_i \eta \pi R_R^2}) (1 - e^{-p_i \eta \pi R_C^2}). \quad (9)$$

*Proof.* By definition, each file  $f_i$  is distributed according to a thinned PPP with spatial density  $p_i \eta$ . Hence, we can straightforwardly infer that the probabilities of  $f_i$  falling independently into the request region  $\mathcal{R}_{d(x)}$  and into the potential cache region  $\mathcal{C}_x$  are  $1 - e^{-p_i \eta \pi R_R^2}$  and  $1 - e^{-p_i \eta \pi R_C^2}$ , respectively. Assume now that  $S \rightarrow \infty$ , i.e., the SBSs are equipped with unlimited storage. Then, in this case, the cache-hit probability of file  $f_i$  can be derived as the probability of file  $f_i$  falling into both the request region and the potential cache region, which is readily given by  $(1 - e^{-p_i \eta \pi R_R^2}) (1 - e^{-p_i \eta \pi R_C^2})$ . Finally, considering the totality of the contents included in the global file catalog  $\mathcal{F}$  and imposing storage constrains from Definition 2 yields the expression in (9).  $\square$

**Remark 4** Note that, in non-cooperative caching settings, the maximization of  $P_{\text{hit}}$  is straightforwardly achieved by caching the  $S$  most popular files at the SBSs.

## 4 Performance Analysis

In this section, we use tools from stochastic geometry to analyze the system-level performance enhancements brought by the considered cache-aided FD network over its cache-free counterpart. This choice provides analytical tractability of the problem and is crucial

to guarantee the generality of our results. As main performance metric, we study the probability that a DL node successfully receives a requested content, either through a direct transmission from its associated SBS or with the aid of the corresponding UL node. We term this metric as *probability of successful transmission*, which is denoted by  $P_{\text{suc}}(\cdot)$ . In this context, it is convenient to recall that the delivery of a requested file will be performed over different links depending on the occurrence of a cache-hit event. In particular:

- *Cache-hit event*: the transmission involves one hop, i.e., from the SBS to the DL node;
- *Cache-miss event*: the transmission requires two hops, i.e., first from the UL node to the SBS and then from the latter to the DL node through the SBS (which introduces additional interference).

In our analysis, we focus on a *typical SBS*, indexed by  $x$ , and its marks  $u(x)$  and  $d(x)$ , referred to as *typical UL node* and *typical DL node*, respectively. Building on Slivnyak's theorem [44, Ch. 8.5] and on the stationarity of  $\Phi_{\text{SBS}}$  (resp. of  $\Phi_{\text{DL}}$ ), the statistics of the typical SBS's (resp. of the typical DL node's) signal reception are representative of the statistics seen by any SBS (resp. by any DL node) in the system.

Switching our focus back to  $P_{\text{suc}}(\cdot)$ , we consider that a requested file is successfully received by the typical DL node (i.e., through the two-hop communication link involving the typical UL node, the typical SBS, and the typical DL node) if  $\text{SIR}_x > \theta \wedge \text{SIR}_{d(x)} > \theta$ , with  $\theta$  defined as a target SIR threshold. Additionally, we consider that the correct reception of the requested file over one hop uniquely depends on the SIR experienced at the receiver, regardless of the considered hop. For simplicity, and without loss of generality, we assume the same SIR threshold for both UL and DL directions.

Now, thanks to the caching capabilities at the typical SBS, we can state that the UL communication does not occur with probability  $P_{\text{hit}}$ . We can then express the probability of successful transmission as

$$P_{\text{suc}}(\theta) \triangleq P_{\text{hit}}\mathbb{P}(\text{SIR}_{d(x)} > \theta) + (1 - P_{\text{hit}})\mathbb{P}(\text{SIR}_x > \theta, \text{SIR}_{d(x)} > \theta). \quad (10)$$

Building upon this definition, other useful performance metrics can be expressed in terms of probability of successful transmission. Noteworthy examples are the outage probability, given by  $P_{\text{out}}(\theta) \triangleq 1 - P_{\text{suc}}(\theta)$ , and the achievable area spectral efficiency (ASE), defined as  $\text{ASE}(\theta) \triangleq \lambda P_{\text{suc}}(\theta) \log_2(1 + \theta)$  (measured in [bps/Hz/m<sup>2</sup>]).

Before proceeding with our analysis, we provide some useful preliminary definitions for the sake of notational simplicity in the remainder of the section:

$$\hat{\Upsilon}(s) \triangleq \frac{\pi(s\rho_{\text{DL}})^{\frac{2}{\alpha_1}} \csc\left(\frac{2\pi}{\alpha_1}\right)}{\alpha_1}, \quad (11)$$

$$\tilde{\Upsilon}(s) \triangleq \int_0^\infty \left(1 - \frac{1}{1 + s\rho_{\text{DL}}r^{-\alpha_1}} \Xi(s, r)\right) r dr, \quad (12)$$

$$\Xi(s, r) \triangleq \frac{1}{2\pi} \int_0^{2\pi} \frac{d\varphi}{1 + s\rho_{\text{UL}}(R_{\text{UL}}^2 + r^2 + 2R_{\text{UL}}r \cos \varphi)^{-\frac{\alpha_2}{2}}}. \quad (13)$$

Recalling the expressions of  $I_x$  and  $I_{d(x)}$  in (3) and (5), respectively, a tight analytical lower bound on  $P_{\text{suc}}(\theta)$  is provided next in Theorem 1, with additional properties given in Corollary 1.

**Theorem 1.** *The probability of successful transmission in (10) is bounded as  $P_{\text{suc}}(\theta) \geq \underline{P}_{\text{suc}}(\theta)$ , with*

$$\underline{P}_{\text{suc}}(\theta) \triangleq P_{\text{hit}} \mathcal{L}_{I_{d(x)}}(\theta \rho_{\text{DL}}^{-1} R_{\text{DL}}^{\alpha_1}) + (1 - P_{\text{hit}}) \mathcal{L}_{I_x}^{\Delta_x}(\theta \rho_{\text{UL}}^{-1} R_{\text{UL}}^{\alpha_1}) \mathcal{L}_{I_{d(x)}}^{\Delta_x}(\theta \rho_{\text{DL}}^{-1} R_{\text{DL}}^{\alpha_1}) \quad (14)$$

where  $\mathcal{L}_{I_{d(x)}}(s)$  is the Laplace transform of the interference observed at DL node  $d(x)$  in case of cache hit, whereas  $\mathcal{L}_{I_x}^{\Delta_x}(s)$  and  $\mathcal{L}_{I_{d(x)}}^{\Delta_x}(s)$  are the Laplace transforms of the interference observed at SBS  $x$  and at DL node  $d(x)$ , respectively, in case of cache-miss:

$$\mathcal{L}_{I_{d(x)}}(s) \triangleq \exp(-2\pi\lambda P_{\text{hit}} \tilde{\Upsilon}(s)) \exp(-2\pi\lambda(1 - P_{\text{hit}}) \tilde{\Upsilon}(s)), \quad (15)$$

$$\mathcal{L}_{I_x}^{\Delta_x}(s) \triangleq \frac{1}{(1 + s\rho_{\text{DL}} b)^a} \mathcal{L}_{I_{d(x)}}(s), \quad (16)$$

$$\mathcal{L}_{I_{d(x)}}^{\Delta_x}(s) \triangleq \Xi(s, R_{\text{DL}}) \mathcal{L}_{I_{d(x)}}(s). \quad (17)$$

*Proof.* The construction of (14) relies on the assumption of uncorrelated locations of the UL and DL nodes in presence of a cache-miss event. As a matter of fact, according to the Fortuin-Kasteleyn-Ginibre (FKG) inequality [44, Ch. 10.4.2], such uncorrelated case yields a lower bound on the network performance for the correlated case (we refer to [25] for further details). Therefore, given  $P_{\text{suc}}(\theta)$  in (10), we can write

$$P_{\text{suc}}(\theta) \geq P_{\text{hit}} P_{\text{suc},2}(\theta) + (1 - P_{\text{hit}}) P_{\text{suc},1}^{\Delta_x}(\theta) P_{\text{suc},2}^{\Delta_x}(\theta) \quad (18)$$

where  $P_{\text{suc},2}(\theta)$  represents the probability of successfully transmitting a requested file from the typical SBS to the typical DL node in case of a cache-hit event, and  $P_{\text{suc},1}^{\Delta_x}(\theta)$  (resp.  $P_{\text{suc},2}^{\Delta_x}(\theta)$ ) denotes the probability of successfully transmitting a requested file from the typical UL node to the typical SBS (resp. from the typical SBS to the typical DL node) in case of a cache-miss event.

We begin by focusing on the latter components, i.e.,  $P_{\text{suc},1}^{\Delta_x}(\theta)$  and  $P_{\text{suc},2}^{\Delta_x}(\theta)$ . In particular,  $P_{\text{suc},1}^{\Delta_x}(\theta)$  is obtained as the Laplace transform of  $I_x$  in (3) in presence of SI [25, Th. 1], which is given by  $\mathcal{L}_{I_x}^{\Delta_x}(s)$  in (16). Likewise,  $P_{\text{suc},2}^{\Delta_x}(\theta)$  is obtained as the Laplace transform of  $I_{d(x)}$  in (5) in presence of INI, which is given by  $\mathcal{L}_{I_{d(x)}}^{\Delta_x}(s)$  in (17). Following a similar approach,  $P_{\text{suc},2}(\theta)$  can be obtained as the Laplace transform of  $I_{d(x)}$  in (5) in absence of INI, which is given by  $\mathcal{L}_{I_{d(x)}}(s)$ . Now, let us define  $\tilde{\Phi}_{\text{SBS}} \triangleq \{x \in \Phi_{\text{SBS}} : \Delta_x\}$  and  $\hat{\Phi}_{\text{SBS}} \triangleq \Phi_{\text{SBS}} \setminus \tilde{\Phi}_{\text{SBS}}$ , which are, by definition, independent PPPs with spatial densities  $P_{\text{hit}}\lambda$  and  $(1 - P_{\text{hit}})\lambda$ , respectively. As a consequence,  $\mathcal{L}_{I_{d(x)}}(s)$  in (15) can be derived as

$$\mathcal{L}_{I_{d(x)}}(s) = \mathbb{E}[e^{-sI_{d(x)}}] \quad (19)$$

$$= \mathbb{E}\left[\exp\left(-s \sum_{y \in \Phi_{\text{SBS}} \setminus \{x\}} (\rho_{\text{DL}} r_{yd(x)}^{-\alpha_1} h_{yd(x)} + \rho_{\text{UL}} r_{u(y)d(x)}^{-\alpha_1} h_{u(y)d(x)} \mathbb{1}_{\Delta_y})\right)\right] \quad (20)$$

$$= \mathbb{E}\left[\prod_{y \in \Phi_{\text{SBS}} \setminus \{x\}} \exp\left(-s(\rho_{\text{DL}} r_{yd(x)}^{-\alpha_1} h_{yd(x)} + \rho_{\text{UL}} r_{u(y)d(x)}^{-\alpha_1} h_{u(y)d(x)} \mathbb{1}_{\Delta_x})\right)\right] \quad (21)$$

$$= \mathbb{E}\left[\prod_{y \in \hat{\Phi}_{\text{SBS}} \setminus \{x\}} \exp\left(-s\rho_{\text{DL}} r_{yd(x)}^{-\alpha_1} h_{yd(x)}\right)\right] \\ \times \mathbb{E}\left[\prod_{y \in \tilde{\Phi}_{\text{SBS}} \setminus \{x\}} \exp\left(-s(\rho_{\text{DL}} r_{yd(x)}^{-\alpha_1} h_{yd(x)} + \rho_{\text{UL}} r_{u(y)d(x)}^{-\alpha_1} h_{u(y)d(x)})\right)\right] \quad (22)$$

and, using the moment-generating function of the exponential distribution, we obtain

$$\mathcal{L}_{I_{d(x)}}(s) = \mathbb{E}_{\hat{\Phi}_{\text{SBS}}}\left[\prod_{y \in \hat{\Phi}_{\text{SBS}} \setminus \{x\}} \frac{1}{1 + s\rho_{\text{DL}} r_{yd(x)}^{-\alpha_1}}\right] \\ \times \mathbb{E}_{\tilde{\Phi}_{\text{SBS}}}\left[\prod_{y \in \tilde{\Phi}_{\text{SBS}} \setminus \{x\}} \frac{1}{1 + s\rho_{\text{DL}} r_{yd(x)}^{-\alpha_1}} \frac{1}{1 + \rho_{\text{UL}} r_{u(y)d(x)}^{-\alpha_1}}\right]. \quad (23)$$

Then, applying the probability generating functional of a PPP [44, Ch. 4.3] yields

$$\mathcal{L}_{I_{d(x)}}(s) = \exp\left(-2\pi\lambda \text{P}_{\text{hit}} \int_0^\infty \left(1 - \frac{1}{1 + s\rho_{\text{DL}} r^{-\alpha_1}}\right) r dr\right) \\ \times \exp\left(-2\pi\lambda (1 - \text{P}_{\text{hit}}) \int_0^\infty \left(1 - \frac{1}{1 + s\rho_{\text{DL}} r^{-\alpha_1}} \Xi(s, r)\right) r dr\right). \quad (24)$$

Finally, the integral appearing in the first exponential of (24) has a closed-form solution given by  $\hat{\Upsilon}(s)$  in (11). This concludes the proof.  $\square$

**Corollary 1.** *The lower bound on the probability of successful transmission in (14) is characterized by the following properties:*

- (a)  $\underline{\text{P}}_{\text{suc}}(\theta) \rightarrow \text{P}_{\text{suc}}(\theta)$  as  $\text{P}_{\text{hit}} \rightarrow 1$ ;
- (b)  $\underline{\text{P}}_{\text{suc}}(\theta) = \text{P}_{\text{suc}}(\theta)$  in case of uncorrelated locations of the nodes between UL and DL communications.

*Proof.* The proof follows directly from Theorem 1.  $\square$

Lastly, we introduce the *FD throughput gain*, which will be used as a performance metric in Section 5, defined as

$$\text{TG}_{\text{FD}}(\theta) \triangleq 2\text{P}_{\text{suc}}(\theta) \exp\left(2\pi\lambda \frac{\pi\theta^{\frac{2}{\alpha_1}} (R_{\text{UL}}^2 + R_{\text{DL}}^2) \csc\left(\frac{2\pi}{\alpha_1}\right)}{\alpha_1}\right). \quad (25)$$

This performance metric quantifies the throughput gain of a cache-aided small-cell network operating in FD mode as compared to its cache-free HD counterpart by relating the

**Table 1** System parameters used in the simulations.

System Parameter	Symbol	Value
Radius of request region	$R_R$	8 m
Radius of potential cache region	$R_C$	40 m
Catalog shape parameter	$\gamma$	0.7
Storage-to-catalog ratio	$\kappa$	{0.1, 0.35, 0.6}
Distance UL node–SBS	$R_{UL}$	20 m
Distance SBS–DL node	$R_{DL}$	5 m
Transmit power of UL nodes	$\rho_{UL}$	30 dBm
Transmit power of DL nodes	$\rho_{DL}$	24 dBm
Pathloss exponent UL nodes–SBSs/SBSs–DL nodes	$\alpha_1$	3
Pathloss exponent UL nodes–DLs nodes	$\alpha_2$	4
Target SIR	$\theta$	0 dB
Rician $K$ -factor	$K$	1
SI attenuation	$\Omega$	60 dB

probability of successful transmission  $P_{\text{suc}}(\theta)$  in the two settings and taking into account the theoretical FD throughput doubling (we refer to [25] for details). In particular, we note that the FD setting outperforms its HD counterpart when  $TG_{\text{FD}}(\theta) > 1$ .

## 5 Numerical Results and Discussion

In this section, we present and discuss numerical results obtained by means of suitable Monte Carlo simulations in order to assess the validity of our theoretical findings. We specifically focus on the analytical expressions obtained in Sections 3 and 4.

As commonly assumed in the literature (see, e.g., [12]), the global file catalog follows a Zipf popularity distribution such that the request probability  $p_i \in \mathcal{P}$  of each file  $f_i \in \mathcal{F}$  can be written as

$$p_i = \left( i^\gamma \sum_{j=1}^F \frac{1}{j^\gamma} \right)^{-1} \quad (26)$$

for a certain catalog shape parameter  $\gamma$ . Hence, the SBSs cache contents from the global file catalog (depending on the policy defined in Definition 2) and serve the corresponding UEs accordingly. The corresponding storage-to-catalog ratio is defined as  $\kappa \triangleq \frac{S}{F} \leq 1$ . The values of the most relevant parameters adopted for the simulations are listed in Table 1; furthermore, the shape parameter  $a$  and the scale parameter  $b$  of the SI distribution,

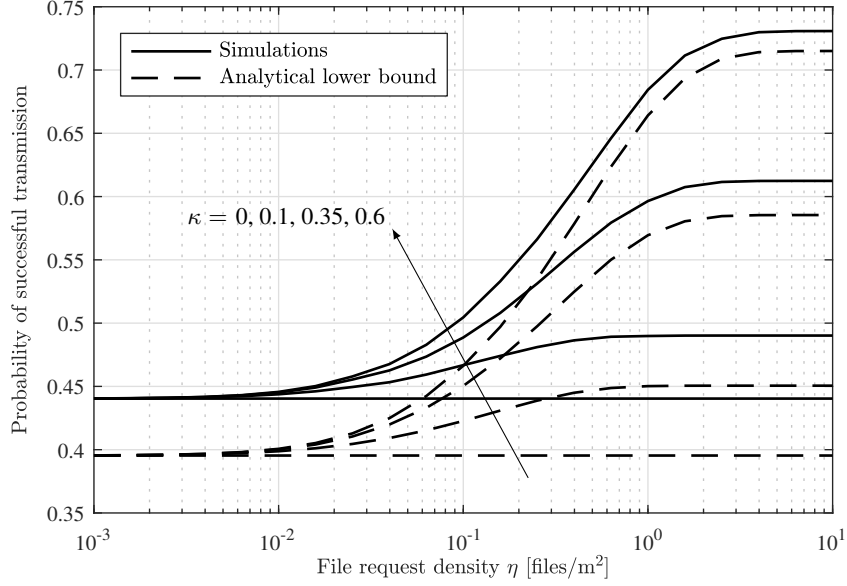


**Fig. 6** Probability of successful transmission against file request density, with SBS density  $\lambda = 5 \times 10^{-4}$  SBSs/m<sup>2</sup>.

which appear in (16), are computed from the Rician  $K$ -factor  $K$  and the SI attenuation  $\Omega$  measured at the FD SBSs as in [25, Lem. 1].

The probability of successful transmission  $P_{\text{suc}}(\theta)$  in (10) and its analytical lower bound  $\underline{P}_{\text{suc}}(\theta)$  in (14) are illustrated in Fig. 6 as functions of the file request density  $\eta$  for a fixed SBS density  $\lambda = 5 \times 10^{-4}$  SBSs/m<sup>2</sup>. With reference to Corollary 1, we recall that  $\underline{P}_{\text{suc}}(\theta)$  gives the exact expression of  $P_{\text{suc}}(\theta)$  for uncorrelated locations of the nodes between UL and DL phases. Moreover, note that the curves for  $\kappa = 0$  are related to the cache-free scenario analyzed in [25] (see also Fig. 7 and Fig. 8). Qualitatively, it is evident from Fig. 6 that the probability of successful transmission grows with both the file request density  $\eta$  and the storage-to-catalog ratio  $\kappa$ . On the one hand, we observe that a higher file request density yields a larger  $P_{\text{hit}}$ , which in turn improves the efficiency of the storage use. On the other hand, the variation experienced by the probability of successful transmission over  $\eta$  increases with the storage capabilities at the SBSs, and so does the tightness of the analytical lower bound. Concerning this last aspect, we note that, even if such bound may look rather loose for  $\kappa \leq 0.35$ , its quantitative difference with the actual numerical performance never exceeds 10%.

Assume now a file request density  $\eta = 1$  files/m<sup>2</sup>. Fig. 7 plots the probability of successful transmission  $P_{\text{suc}}(\theta)$  in (10) and its analytical lower bound  $\underline{P}_{\text{suc}}(\theta)$  in (14) as functions of the SBS density  $\lambda$ . The analytical lower bound is remarkably tight and, in accordance with Fig. 6, becomes increasingly accurate as the storage-to-catalog ratio  $\kappa$  grows. Nonetheless, it is even more meaningful to analyze the FD throughput gain in (25) together with its analytical lower bound (obtained by replacing  $P_{\text{suc}}(\theta)$  with  $\underline{P}_{\text{suc}}(\theta)$  in



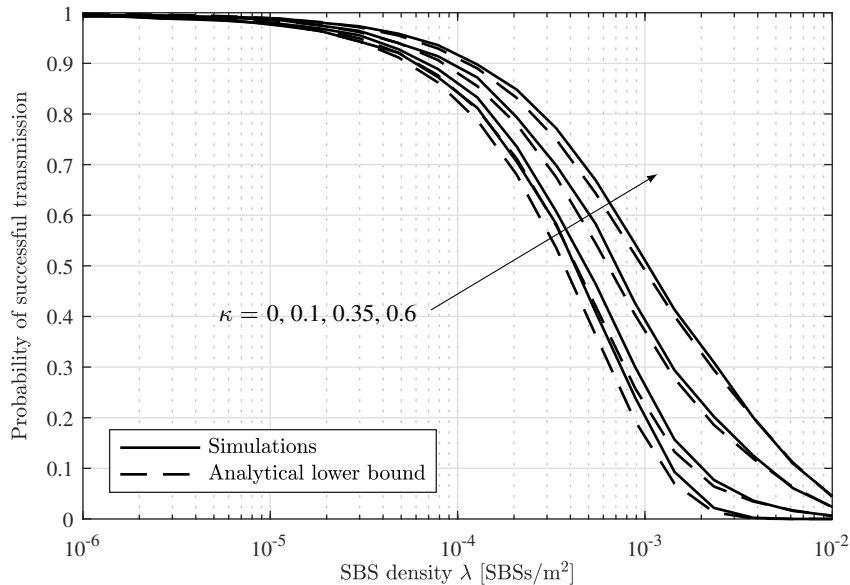


**Fig. 7** Probability of successful transmission against SBS density, with file request density  $\eta = 1$  files/m<sup>2</sup>.

the aforementioned expression), which are illustrated in Fig. 8 against the SBS density  $\lambda$ . In practice, higher ASE can be achieved by deploying a very dense FD network in which each SBS is equipped with suitable caching capabilities. In this respect, we observe that:

- a SBS density  $\lambda = 10^{-4}$  SBSs/m<sup>2</sup> yields  $TG_{FD}(\theta) = 1.7$  with  $\kappa = 0$  and  $TG_{FD}(\theta) = 1.85$  with  $\kappa = 0.6$ ;
- a SBS density  $\lambda = 10^{-3}$  SBSs/m<sup>2</sup> yields  $TG_{FD}(\theta) = 0.42$  with  $\kappa = 0$  and  $TG_{FD}(\theta) = 1.11$  with  $\kappa = 0.6$ .

It is evident that the optimal tradeoff between the SBS density and the storage size installed at each SBS must be found by network planners taking into account the deployment cost of each element; the interested reader may refer to [16] for further details on this subject.

## 6 Conclusions

Several research efforts in both academic and industrial contexts have highlighted that edge caching can provide significant benefits in terms of network performance as, e.g., end-to-end access delay. Conversely, very few straightforward insights can be drawn on the benefits experienced at the physical layer when the network nodes are equipped with caching capabilities. This is mostly due to the complexity of the physical interactions occurring among devices in modern network.

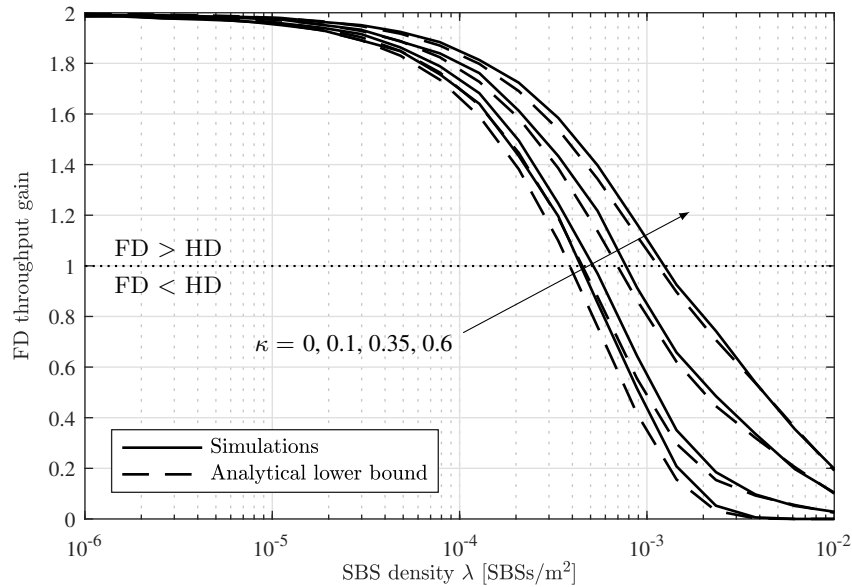


**Fig. 8** FD throughput gain against SBS density, with file request density  $\eta = 1$  files/m<sup>2</sup>.

This chapter takes a step forward with respect to the aforementioned position by showing that edge caching can actually offer a remarkable degree of interoperability with one of the most promising technologies for next-generation network deployments, i.e., FD communications. More specifically, we show that integrating caching capabilities at the FD SBSs is a cost-effective means of improving the scalability of the theoretical throughput doubling brought by the FD paradigm from the device to the network level.

Our study considers an interference-limited UDN setting consisting of several non-cooperative SBSs with FD capabilities, which simultaneously communicate with both their served UEs and wireless BNs. In this case, the interference footprint of the UDN, already significant by design, is further increased by the FD operations. In fact, the latter induce higher levels of inter-cell and inter-node interference as compared to the HD scenario, in turn causing a spectral efficiency bottleneck that prevents the theoretical FD throughput doubling to occur at the network level. Fundamental results available in the literature show that most of such doubling can be achieved only if the network infrastructure is subject to radical and expensive modifications or if high-rate signaling is exchanged between UEs over suitable control links.

In this context, we add file storage capabilities to SBSs and consider a geographical caching policy aiming at capturing local files popularity, whereby the SBSs intelligently store popular contents anticipating the UEs' requests. The rationale of this choice is that the presence of pre-fetched popular files at the SBSs reduces the need for the latter to retrieve contents from the wireless BNs upon the UEs' request. This clearly diminishes the number of transmissions performed by the BNs towards the SBSs, in turn reducing the

interference footprint of the UDN. Remarkably, this low-cost solution can be implemented without the need for additional signaling between the nodes or any infrastructural change.

The performance of such cache-aided FD network is characterized in terms of throughput gain as compared to its HD counterpart. To this end, two fundamental metrics are identified and analyzed:

- The cache-hit probability, defined as the probability that any file requested by a given UE from its serving SBS is cached at the latter;
- The probability of successful transmission of a file requested by a UE, either directly by its serving SBS (if present in its cache) or by the corresponding BN.

In particular, the second metric is used to derive an analytical lower bound on the throughput of the UDN. As a final step, we perform a set of suitable numerical simulations to assess the performance enhancement brought by the adoption of edge caching. The obtained results highlight that shifting from cache-free to cache-aided UDNs allows to effectively operate the network in FD mode while supporting higher SBS densities, in turn improving the ASE. In other words, the deployment of cache-aided SBSs has beneficial effects on the network throughput experienced over a given area, thanks to a non-negligible reduction of the aggregate interference observed in the FD network in comparison with the cache-free case.

The results presented in this chapter demonstrate that the interoperability between edge caching and FD communications is not only possible, but also desirable from the network throughput perspective. However, from a quantitative point of view, the extent of the benefits may strongly depend on several parameters, such as:

- Adopted caching policy;
- UEs association policy;
- Mobility of the network nodes, either in the form of moving SBSs or classic UEs' dynamics.

Therefore, future additional studies and investigations should be performed in these directions to further deepen our understanding of the benefits brought by edge caching to the physical layer of wireless communication networks, especially when the FD paradigm is adopted.

## Acknowledgments

The work of Italo Atzeni was supported by the European Research Council under the Horizon 2020 Programme (ERC 670896 PERFUME).

## References

1. Cisco, “Cisco Visual Networking Index: Global Mobile Data Traffic Forecast, 2016–2021,” *White Paper*, 2017.
2. J. G. Andrews, S. Buzzi, W. Choi, S. V. Hanly, A. Lozano, A. C. K. Soong, and J. C. Zhang, “What will 5G be?” *IEEE J. Sel. Areas Commun.*, vol. 32, no. 6, pp. 1065–1082, June 2014.
3. 3GPP, “TR 38.211 (V15.1.0): NR; physical channels and modulation,” Tech. Rep., Mar. 2018.
4. —, “TR 38.214 (V15.1.0): NR; physical layer procedures for data,” Tech. Rep., Mar. 2018.
5. F. Boccardi, R. W. Heath, A. Lozano, T. L. Marzetta, and P. Popovski, “Five disruptive technology directions for 5G,” *IEEE Commun. Mag.*, vol. 52, no. 2, pp. 74–80, Feb. 2014.
6. E. Björnson, J. Hoydis, and L. Sanguinetti, “Massive MIMO networks: Spectral, energy, and hardware efficiency,” *Foundations and Trends in Signal Process.*, vol. 11, no. 3–4, pp. 154–655, 2017.
7. E. Baştuğ, M. Bennis, M. Kountouris, and M. Debbah, “Cache-enabled small cell networks: modeling and tradeoffs,” *EURASIP J. Wireless Commun. Netw.*, no. 1, pp. 41–51, 2015.
8. K. Li, C. Yang, Z. Chen, and M. Tao, “Optimization and analysis of probabilistic caching in  $n$ -tier heterogeneous networks,” *IEEE Trans. Wireless Commun.*, vol. 17, no. 2, pp. 1283–1297, Feb. 2018.
9. K. Hamidouche, W. Saad, M. Debbah, and H. V. Poor, “Mean-field games for distributed caching in ultra-dense small cell networks,” in *Proc. IEEE American Control Conf. (ACC)*, Boston, MA, USA, Jul. 2016.
10. C. Yang, B. Xia, W. Xie, K. Huang, Y. Yao, and Y. Zhao, “Interference cancellation at receivers in cache-enabled wireless networks,” *IEEE Trans. Veh. Technol.*, vol. 67, no. 1, pp. 842–846, Jan. 2018.
11. S. Krishnan and H. S. Dhillon, “Effect of user mobility on the performance of device-to-device networks with distributed caching,” vol. 6, no. 2, pp. 194–197, Apr. 2017.
12. G. Paschos, E. Baştuğ, I. Land, G. Caire, and M. Debbah, “Wireless caching: technical misconceptions and business barriers,” *IEEE Commun. Mag.*, vol. 54, no. 8, pp. 16–22, Aug. 2016.
13. D. Liu and C. Yang, “Caching policy toward maximal success probability and area spectral efficiency of cache-enabled HetNets,” *IEEE Trans. Commun.*, vol. 65, no. 6, pp. 2699–2714, June 2017.
14. A. Khreishah, J. Chakareski, and A. Gharaibeh, “Joint caching, routing, and channel assignment for collaborative small-cell cellular networks,” *IEEE J. Sel. Areas Commun.*, vol. 34, no. 8, pp. 2275–2284, Aug. 2016.
15. M. Maso, I. Atzeni, I. Ghamnia, E. Baştuğ, and M. Debbah, “Cache-aided full-duplex small cells,” in *Proc. Int. Symp. Modeling and Optimiz. in Mobile, Ad Hoc, and Wireless Netw. (WiOpt)*, Paris, France, May 2017.
16. I. Atzeni, M. Maso, I. Ghamnia, E. Baştuğ, and M. Debbah, “Flexible cache-aided networks with backhauling,” in *Proc. IEEE Int. Workshop Signal Process. Adv. Wireless Commun. (SPAWC)*, Sapporo, Japan, July 2017.
17. J. G. Andrews, F. Baccelli, and R. K. Ganti, “A tractable approach to coverage and rate in cellular networks,” *IEEE Trans. Commun.*, vol. 59, no. 11, pp. 3122–3134, Nov. 2011.
18. H. S. Dhillon, R. K. Ganti, F. Baccelli, and J. G. Andrews, “Modeling and analysis of  $K$ -tier downlink heterogeneous cellular networks,” *IEEE J. Sel. Areas Commun.*, vol. 30, no. 3, pp. 550–560, Apr. 2012.
19. S. F. Yunas, M. Valkama, and J. Niemelä, “Spectral and energy efficiency of ultra-dense networks under different deployment strategies,” *IEEE Commun. Mag.*, vol. 53, no. 1, pp. 90–100, Jan. 2015.
20. E. Baştuğ, M. Bennis, and M. Debbah, “Living on the Edge: The role of proactive caching in 5G wireless networks,” *IEEE Commun. Mag.*, vol. 52, no. 8, pp. 82–89, Aug. 2014.
21. A. Sabharwal, P. Schniter, D. Guo, D. W. Bliss, S. Rangarajan, and R. Wichman, “In-band full-duplex wireless: Challenges and opportunities,” *IEEE J. Sel. Areas Commun.*, vol. 32, no. 9, pp. 1637–1652, Sept. 2014.
22. I. Atzeni and M. Kountouris, “Full-duplex MIMO small-cell networks: Performance analysis,” in *Proc. IEEE Global Commun. Conf. (GLOBECOM)*, San Diego, CA, USA, Dec. 2015.
23. Z. Tong and M. Haenggi, “Throughput analysis for full-duplex wireless networks with imperfect self-interference cancellation,” *IEEE Trans. Commun.*, vol. 63, no. 11, pp. 4490–4500, Nov. 2015.
24. S. Goyal, P. Liu, S. S. Panwar, R. A. Difazio, R. Yang, and E. Bala, “Full duplex cellular systems: Will doubling interference prevent doubling capacity?” *IEEE Commun. Mag.*, vol. 53, no. 5, pp. 121–127, May 2015.

25. I. Atzeni and M. Kountouris, "Full-duplex MIMO small-cell networks with interference cancellation," *IEEE Trans. Wireless Commun.*, vol. 16, no. 12, pp. 8362–8376, Dec. 2017.
26. M. Maso, C.-F. Liu, C.-H. Lee, T. Q. S. Quek, and L. S. Cardoso, "Energy-recycling full-duplex radios for next generation networks," *IEEE J. Sel. Areas Commun.*, vol. 33, no. 12, pp. 2948–2962, Dec. 2015.
27. M. Duarte, C. Dick, and A. Sabharwal, "Experiment-driven characterization of full-duplex wireless systems," *IEEE Trans. Wireless Commun.*, vol. 11, no. 12, pp. 4296–4307, Dec. 2012.
28. D. Bharadia, E. McMillin, and S. Katti, "Full duplex radios," *ACM SIGCOMM Comput. Commun. Review*, vol. 43, no. 4, pp. 375–386, Aug. 2013.
29. D. Bharadia and S. Katti, "Full duplex MIMO radios," in *Proc. USENIX Symp. Netw. Syst. Design and Implementation (NSDI)*, Seattle, WA, USA, Apr. 2014.
30. J. I. Choi, M. Jain, K. Srinivasan, P. Levis, and S. Katti, "Achieving single channel, full duplex wireless communication," in *Proc. Ann. Int. Conf. Mobile Computing and Netw. (MOBICOM)*, Chicago, IL, USA, Sept. 2010.
31. M. E. Knox, "Single antenna full duplex communications using a common carrier," in *Proc. IEEE Ann. Wireless and Microw. Technology Conf. (WAMICON)*, Cocoa Beach, FL, USA, Apr. 2012.
32. D. Bharadia, K. Joshi, and S. Katti, "Robust full duplex radio link," *ACM SIGCOMM Comput. Commun. Review*, vol. 44, no. 4, pp. 9147–148, Aug. 2014.
33. N. Phungamngern, P. Uthansakul, and M. Uthansakul, "Digital and RF interference cancellation for single-channel full-duplex transceiver using a single antenna," in *Int. Conf. Elect. Eng./Electron., Comput., Telecommun. and Inf. Technology (ECTI-CON)*, Krabi, Thailand, May 2013.
34. M. Jain, J. I. Choi, T. Kim, D. Bharadia, S. Seth, K. Srinivasan, P. Levis, S. Katti, and P. Sinha, "Practical, real-time, full duplex wireless," in *Proc. Ann. Int. Conf. Mobile Computing and Netw. (MOBICOM)*, Las Vegas, NV, USA, Sept. 2011.
35. N. Li, W. Zhu, and H. Han, "Digital interference cancellation in single channel, full duplex wireless communication," in *Proc. Int. Conf. Wireless Commun., Netw. and Mobile Computing (WiCOM)*, Shanghai, China, Sept. 2012.
36. E. Ahmed and A. Eltawil, "All-digital self-interference cancellation technique for full-duplex systems," *IEEE Trans. Wireless Commun.*, vol. 14, no. 7, pp. 3519–3532, Jul. 2015.
37. D. Korpi, L. Anttila, and M. Valkama, "Reference receiver based digital self-interference cancellation in MIMO full-duplex transceivers," in *Proc. IEEE Global Commun. Conf. (GLOBECOM)*, Austin, TX, USA, Dec. 2014.
38. I. Atzeni, M. Maso, and M. Kountouris, "Optimal low-complexity self-interference cancellation for full-duplex MIMO small cells," in *Proc. IEEE Int. Conf. Commun. (ICC)*, Kuala Lumpur, Malaysia, May 2016.
39. G. C. Alexandropoulos, M. Kountouris, and I. Atzeni, "User scheduling and optimal power allocation for full-duplex cellular networks," in *Proc. IEEE Int. Workshop Signal Process. Adv. Wireless Commun. (SPAWC)*, Edinburgh, UK, July 2016.
40. I. Atzeni, M. Kountouris, and G. C. Alexandropoulos, "Performance evaluation of user scheduling for full-duplex small cells in ultra-dense networks," in *European Wireless (EW) Conf.*, Oulu, Finland, May 2016.
41. S. Wang, V. Venkateswaran, and X. Zhang, "Fundamental analysis of full-duplex gains in wireless networks," *IEEE/ACM Trans. Netw.*, vol. 25, no. 3, pp. 1401–1416, June 2017.
42. L. Wang, F. Tian, T. Svensson, D. Feng, M. Song, and S. Li, "Exploiting full duplex for device-to-device communications in heterogeneous networks," *IEEE Commun. Mag.*, vol. 53, no. 5, pp. 146–152, May 2015.
43. J. Bai and A. Sabharwal, "Distributed full-duplex via wireless side-channels: Bounds and protocols," *IEEE Trans. Wireless Commun.*, vol. 12, no. 8, pp. 4162–4173, Aug. 2013.
44. M. Haenggi, *Stochastic Geometry for Wireless Networks*. New York, NY, USA: Cambridge University Press, 2012.
45. I. Atzeni, J. Arnau, and M. Kountouris, "Downlink cellular network analysis with LOS/NLOS propagation and elevated base stations," *IEEE Trans. Wireless Commun.*, vol. 17, no. 1, pp. 142–156, Jan. 2018.
46. 3GPP, "TR 36.828 (V11.0.0): Further enhancements to LTE time division duplex (TDD) for downlink-uplink (DL-UL) interference management and traffic adaptation," Tech. Rep., Jun. 2012.